RSC Advances

PAPER

View Article Online
View Journal | View Issue

Cite this: *RSC Adv.*, 2020, **10**, 18694

Laser direct writing of carbonaceous sensors on cardboard for human health and indoor environment monitoring†

Kuan Ju,[a] Yang Gao,*[a] Ting Xiao,[a] Cunjiang Yu,[b] Jianpin Tan[a] and Fuzhen Xuan*[a]

Paper-based sensing platforms hold promise in human physiological health monitoring, soft robots, and indoor environment monitoring, owing to their cost effectiveness, flexibility, disposability, and biodegradability. However, most of the existing paper-based sensors require complex fabrication procedures which are also associated with high-cost. Herein, we report a simple yet effective manufacturing process of paper-based carbonaceous sensors based on a laser direct writing (LDW) method. Specifically, carbonaceous pressure, temperature, and humidity sensors on cardboard are developed for human physiological signal monitoring and indoor environment monitoring. Due to the external force induced compaction of the layered carbon flakes, the LDW pressure sensor array has a sensitivity of $\sim -0.563\ kPa^{-1}$, a broad sensing range (0.009–50 kPa), and a high mechanical durability (over 11 000 cycles), all of which are promising for human health monitoring. The LDW-temperature and humidity devices have sensitivities of −0.002/°C and 36.75 fF per % RH, respectively. A prototype is developed using cardboard integrated with temperature and humidity sensors, which not only serves as an ornament to decorate homes but also works as a sensor platform for indoor environment monitoring. Systematic investigation of the LDW manufacturing process, sensing mechanisms, and sensor design and evaluation illustrates the key aspects of carbonaceous sensors.

Received 10th March 2020
Accepted 5th May 2020

DOI: 10.1039/d0ra02217a

rsc.li/rsc-advances

1. Introductions

Sensors, which electrically convert physical and/or chemical parameters into readable signals, have versatile applications in soft robots,[1] electronic skins,[2] indoor environment monitoring,[3] and human–machine interfaces.[4] For instance, electronic skins integrated with pressure or strain sensors are able to convert mechanical deformations into piezoresistive,[5] piezoelectric,[6] capacitive,[7] or transistor signals,[3,8] and are promising for detecting health-related bio-signals including pulse rate, articular motion, and intraocular pressure for health diagnosis.[9] Indoor environmental factors, especially thermal comfort and humidity, critically affect human quality of life. Indoor health monitoring devices equipped with temperature and humidity sensors can assist the indoor environment control system in providing a comfortable physical environment for humans, reducing the physiological stress influencing human health.[10] To achieve these applications mentioned above, not only should the sensors have high sensitivity, rapid response speed, and mechanical robustness,[11] but they should also be developed with a highly efficient and scalable fabrication method.

As a low-cost, flexible, disposable, and degradable substrate material, paper has been employed as the platform for constructing various devices ranging from energy storage modules,[12] biosensors to electronics.[13] Nanomaterials including, but not limited to, carbon nanotubes,[14] graphene,[15] metal nanowires,[16] and MXene,[17] have been successfully employed to construct a variety of sensors on paper using fabrication techniques such as screen printing,[18] inkjet printing,[19] and three-dimensional printing.[20] Although promising device performance has been achieved based on these methods, challenges exist including poor scalability, time-consuming and complex procedures, or cost-ineffectiveness.[21,22] For instance, screen printing, inkjet printing, and three-dimensional printing have the capability to fabricate sensors with high scalability and efficiency. Nevertheless, to prepare the inks with desired conductivity and viscosity is generally time-consuming and technically challenging.[23] Additionally, the indispensable additive used to make the inks might poison the active material and lead to inferior sensing performance.

As a scalable and highly-efficient technique, laser direct writing (LDW) has been used for fabricating electronic devices. Through the programmed laser spot movements, functional material preparation and patterning can be achieved simultaneously, and

[a]School of Mechanical and Power Engineering, East China University of Science and Technology, Shanghai 200237, China. E-mail: yanggao@ecust.edu.cn; fzxuan@ecust.edu.cn

[b]Department of Mechanical Engineering, University of Houston, Houston, TX 77204,, USA

† Electronic supplementary information (ESI) available. See DOI: 10.1039/d0ra02217a

thus facilitate the preparation of devices such as various sensors[24] and energy storage devices.[25] In specific, an LDW method was developed by Ren *et al.*[26,27] to prepare flexible sensors for the application of electronic skin. LDW was used to convert oxidized graphene into reduced graphene, followed by a post-LDW process to remove untreated oxidized graphene and obtain the final device. Different from Ren's method, Luo[28] and Ziaie's[29] group reported the LDW of sensors on polyimide substrates. Since LDW directly converts polyimide into the active material of carbon, no precursor is required. Similarly, our group[30] reported the fabrication of flexible SiC-based strain sensors through direct LDW which converted polydimethylsiloxane into a functional material. Wu *et al.* successfully manufactured a transparent heated glass by LDW fabrication of graphene resistors on the glass.[31] These studies proved the capability of LDW for highly efficient and scalable sensor fabrication. Moreover, LDW can be applied as a mask-less method for fabricating devices on paper since the main component of paper is cellulose fibers, which can serve as a precursor material for sensor development.

As a disposable packaging material, cardboard is widely used in daily life. Although cardboard is used for storage, recycling, and other recreational purposes, it could also be integrated with sensing functionalities for monitoring physiological signals and the indoor environment. Various printing techniques[18–20] could be employed to prepared sensors on cardboard. Nevertheless, the conductive inks should have optimized viscosity to prevent the spread or smudge of the inks on the cardboard during printing which leads to the poor patterning and inferior device performance. In this work, a LDW technique was developed for the fabrication of carbonaceous sensors on cardboard for human physiological signal monitoring and indoor environment monitoring. In contrast to the printing technique, neither conductive inks nor external precursors are needed during the device fabrication in LDW, since cardboard is made from cellulose fibers,[32] which provides the carbon sources for various type of sensors.[33,34] LDW of carbonaceous sensors, including pressure, temperature, and humidity sensors was investigated. LDW-pressure sensor arrays have a layered porous structure. The loading-induced porosity reduction and the conductivity improvement provides a sensitivity of $-0.563\ \mathrm{kPa}^{-1}$ to the device with a sensing range from 0.009 to 50 kPa, and a good mechanical stability for 11 000 cycles, showing an ability to detect various stimuli including pulse rate and muscle movement. The temperature and humidity sensors fabricated by LDW show a sensitivity of $-0.003/^{\circ}\mathrm{C}$ and 36.75 fF per %RH, respectively. Cardboard having LDW-cartoon images and LDW-sensors for temperature and humidity monitoring not only can be applied as an ornament to decorate the house but also work as a sensor platform for indoor environment monitoring.

2. Experimental section

Preparation of the cardboard

The cardboard (fabricated by Sichuan Guangan Hangrui Paper Products Co. Ltd.) was firstly cut into small squares. The Dragon Skin-10 (SMOOTH-ON) which is a high-performance platinum-cured liquid silicone compound, was used as the elastomer substrate. Part A and B of the Dragon Skin were mixed in a ratio of 1 : 1 and were poured onto the cardboard surface. The mixture was cured at 60 °C for 30 min in a vacuum drying oven (Shanghai Yuejin Medical Instruments).

LDW of carbonaceous patterns on cardboard

Carbonaceous patterns were prepared by an open-air LDW technique. The experiment setup included a 532 nm continuous wave laser (Verdi G10, Coherent, Inc), a focusing objective, a dichroic filter, mirrors, and a 3D translational platform (PSA150-11-X, Zolix Inc). The laser beam with a beam size of ~18 μm irradiated on cardboard through the guidance of the optical assembly. The carbonaceous patterns were realized on the cardboard by programming the movements of the 3D translational platform. The laser power and scanning speed were optimized to be 0.2–0.4 W and 15 mm s^{-1}, respectively, for synthesizing carbonaceous patterns.

LDW of pressure, temperature, and humidity sensors

The carbonaceous pressure, temperature, and humidity sensors were fabricated using the same experimental parameters for the carbonaceous patterns. The pressure sensors have a device configuration with LDW-induced interdigitated electrodes at the bottom covered by an LDW-induced carbonaceous film. The resistive temperature sensors have a serpentine configuration. The humidity sensors operating in capacitive mode have LDW-induced interdigitated electrodes deposited with a layer of poly(vinyl alcohol) (PVA). The PVA concentration was 2 wt%. For all the LDW-fabricated carbonaceous sensors, carbon fibers serving as the current collectors were attached to the electrodes by carbon grease (MG Chemical Inc.) for characterization.

Characterization of the LDW-induced carbon on cardboard

The morphologies of the LDW-induced carbon were studied by a transmission electron microscope (TEM, JEM-2100, JEOL) and a field-emission scanning electron microscope (FE-SEM, Hitachi S-4800). The crystallinity and chemical composition of the LDW-synthesized carbon were studied using a micro-Raman spectroscope (Renishaw Invia) with an excitation laser (514 nm) and X-ray photoelectron spectroscopy (XPS, Thermo Fisher spectrometer, ESCALAB 250).

Characterization of the LDW sensors

The sensing performance of the pressure sensor was characterized with an electrochemical workstation (CHI660E, Shanghai Chenhua Instruments). The applied pressure was loaded by a Mark-10 force meter on a motorized test stand (ESM303, Mark-10 Inc.). The sensitivity (S_p) of the device was calculated by:

$$S_p = \frac{\Delta R_p / R_{po}}{\Delta P} \quad (1)$$

where ΔP, R_{po}, and ΔR_p are the applied pressure, the device's initial resistance without loading, and the resistance change caused by the loading of ΔP, respectively.

The characteristics of the 3 × 3 pressure sensor array were investigated with an Arduino electronic platform based graphic control interface and the electrochemical workstation.

The thermo-responsivity of the temperature sensor was measured with the electrochemical workstation. During the measurement, the sensor was heated to different temperatures using a heater (IKA C-Mag HS7). The sensitivity (S_T) of the temperature sensor is defined as follows:

$$S_T = \frac{R_t - R_0}{R_0(T_t - T_0)} \quad (2)$$

where T_t and T_0 are the initial and target temperatures, respectively; R_t and R_0 denote the resistances of the device at T_t and T_0, respectively.

An LCR meter (IM 3536 LCR METER, HIOKI) was used to record the humidity sensor's capacitance under different humidities. The humidity was controlled and measured by humidifier and humidity meter, respectively. The sensitivity (S_H) of the humidity sensor is given as follows:

$$S_H = \frac{C_t - C_0}{\Delta RH} \quad (3)$$

where C_t and C_0 are the capacitances of the sensor at the target and initial humidity, respectively; ΔRH represents the variation of the testing humidity.

3. Results and discussion

LDW of conductive carbonaceous layers on cardboard

Cardboard is made from cellulose fiber with layered paper pressed together, which provides the carbon sources for the LDW fabrication of various patterns and different type of sensors. Fig. 1a illustrates the system developed in our group for the LDW in the open air. A piece of cardboard was irradiated by a laser beam (532 nm) guided by an optical assembly having mirrors, a dichroic

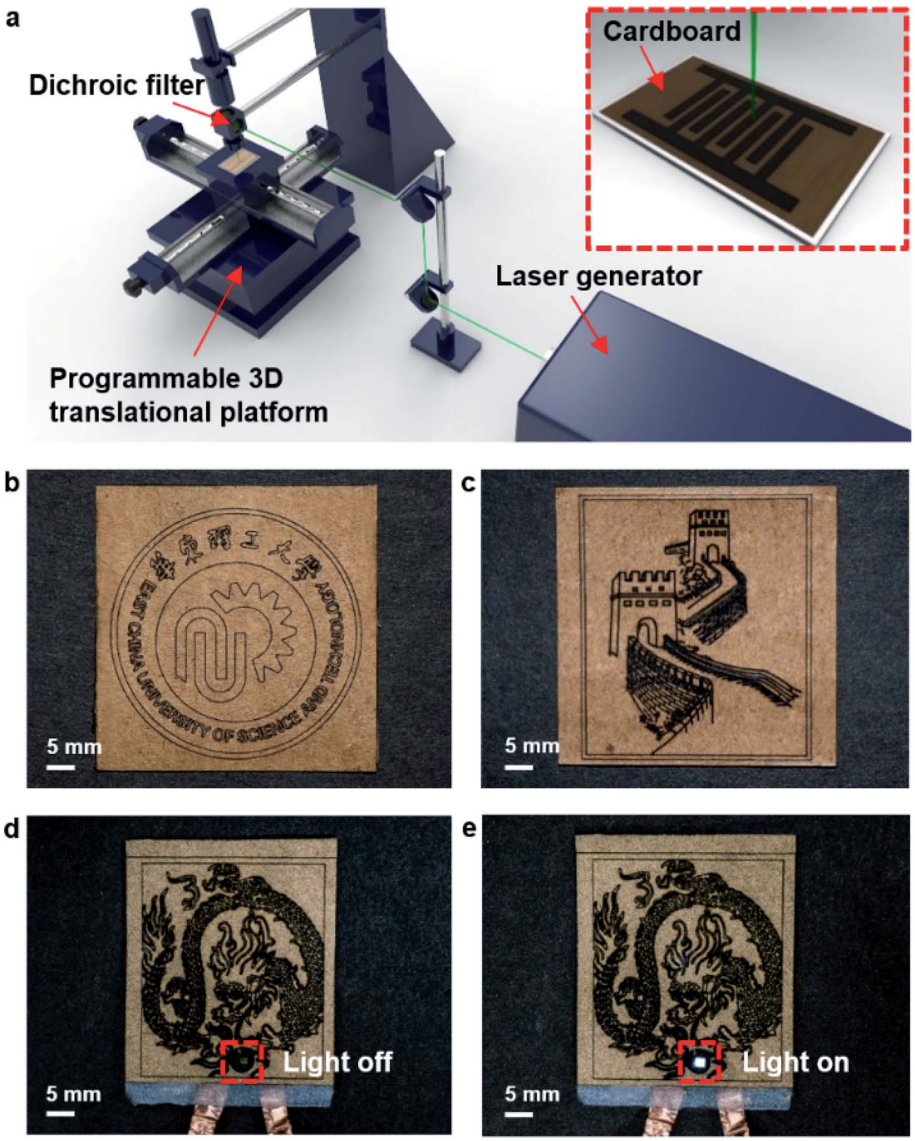

Fig. 1 LDW of conductive carbonaceous layers on cardboard. (a) A schematic diagram exhibiting the LDW fabrication of the carbonized cardboard sensor. Photographs showing LDW-prepared patterns of (b) a logo of the East China University of Science and Technology, (c) the Great Wall, (d) a Chinese dragon with the LED off, and (e) the Chinese dragon with the LED on.

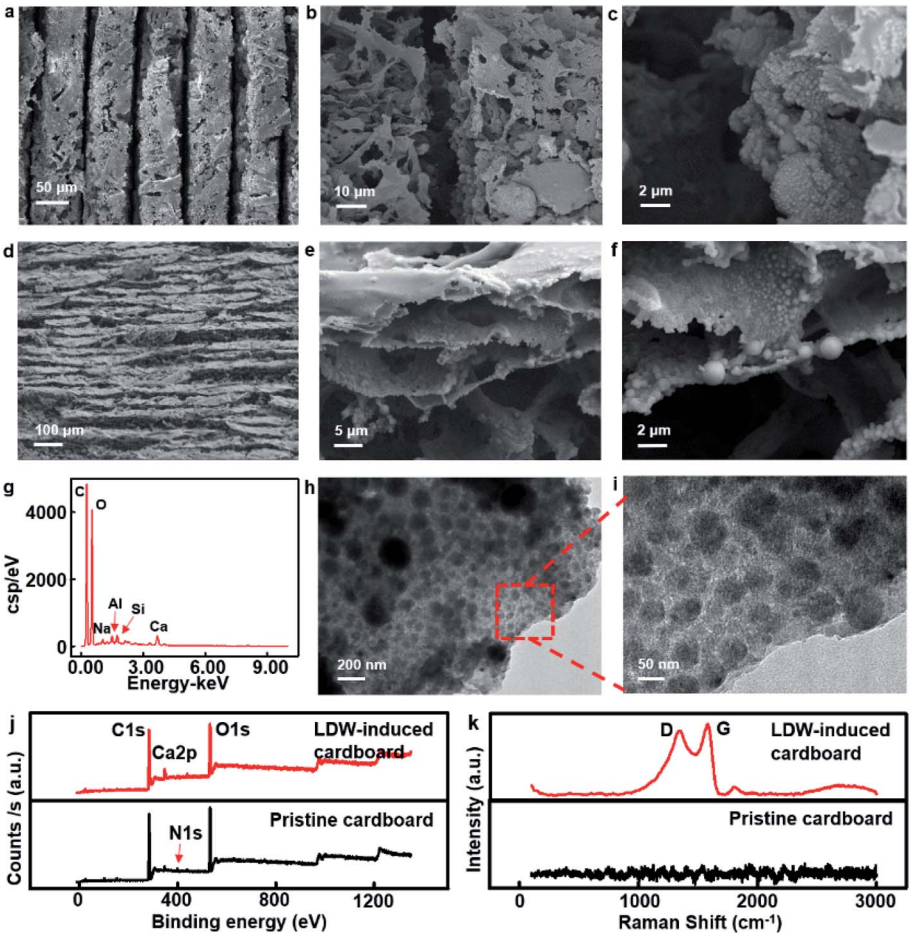

Fig. 2 Systematical characterization of the LDW-induced conductive carbon on the cardboard. (a–c) SEM images of the LDW-carbonized cardboard obtained at 0.4 W. (d–f) Cross-sectional SEM images of the LDW-carbonized cardboard obtained at 0.4 W. (g) The EDS spectrum of the LDW-carbonized cardboard. (h and i) TEM images of the LDW carbonized cardboard obtained at 0.4 W. (j) XPS spectra of the pristine cardboard and the LDW-carbonized cardboard at 0.4 W. (k) Raman spectra of the pristine cardboard and the LDW-carbonized cardboard at 0.4 W.

filter, and a focusing objective. Through the programmed movement of a 3D translational platform, the carbonization and patterning processes can be accomplished in one step, as proven by the different conductive carbon patterns, such as the logo of East China University of Science and Technology (Fig. 1b), the Great Walls of China (Fig. 1c), and the Chinese Dragon (Fig. 1d) synthesized on the cardboard. Cardboard has been repurposed for recreational uses, such as photo frames, indoor dog houses, or dollhouses for children. The LDW makes the cardboard suitable as an ornament for homes, since various patterns could be scalably and efficiently generated on it. However, the LDW pattern on cardboard not only can serve as an ornament, but also can be used to develop functional electronic devices. At a fixed scanning speed of 15 mm s^{-1}, the LDW-induced carbon is conductive at laser powers from 0.2 to 0.4 W (Fig. S1a and b†). The increased laser power can improve the conductivity of the carbonaceous patterns, with the highest conductivity obtained at 0.4 W. As a demonstration, the Chinese Dragon pattern was used as a conductor to illuminate a light emitting diode, as shown in Fig. 1e.

Characterization of the LDW-carbonized cardboard

Systematical characterization was performed to study the morphologies, chemical composition, and quality of the LDW-induced conductive carbon on the cardboard. The primary raw material used to make cardboard is the pine tree, which typically has long fibers and grows rapidly. Cardboard is generally coated with additive pigments to improve the surface and optical properties.[35,36] Pigments are usually derived from various minerals, such as kaolin clay, calcium carbonate, and titanium dioxide. Fig. S2a–c† illustrates the surface morphology of the cardboard before LDW processing. Cellulose fibers with different sizes are observed to be intertwined together (Fig. S2a–c†). Fig. S2d–f† shows the cross-sectional morphology of the pristine cardboard and cellulose fibers and calcium carbonate agglomerates are observed. The LDW process dramatically changes the morphology of the cardboard. The morphology of the LDW-induced conductive carbon is shown in the FE-SEM images of Fig. 2a–c. During the LDW processing, grooves with a width of 15–20 μm were formed on the surface of the cardboard, as shown in Fig. 2a. Although the laser beam spot is ~18

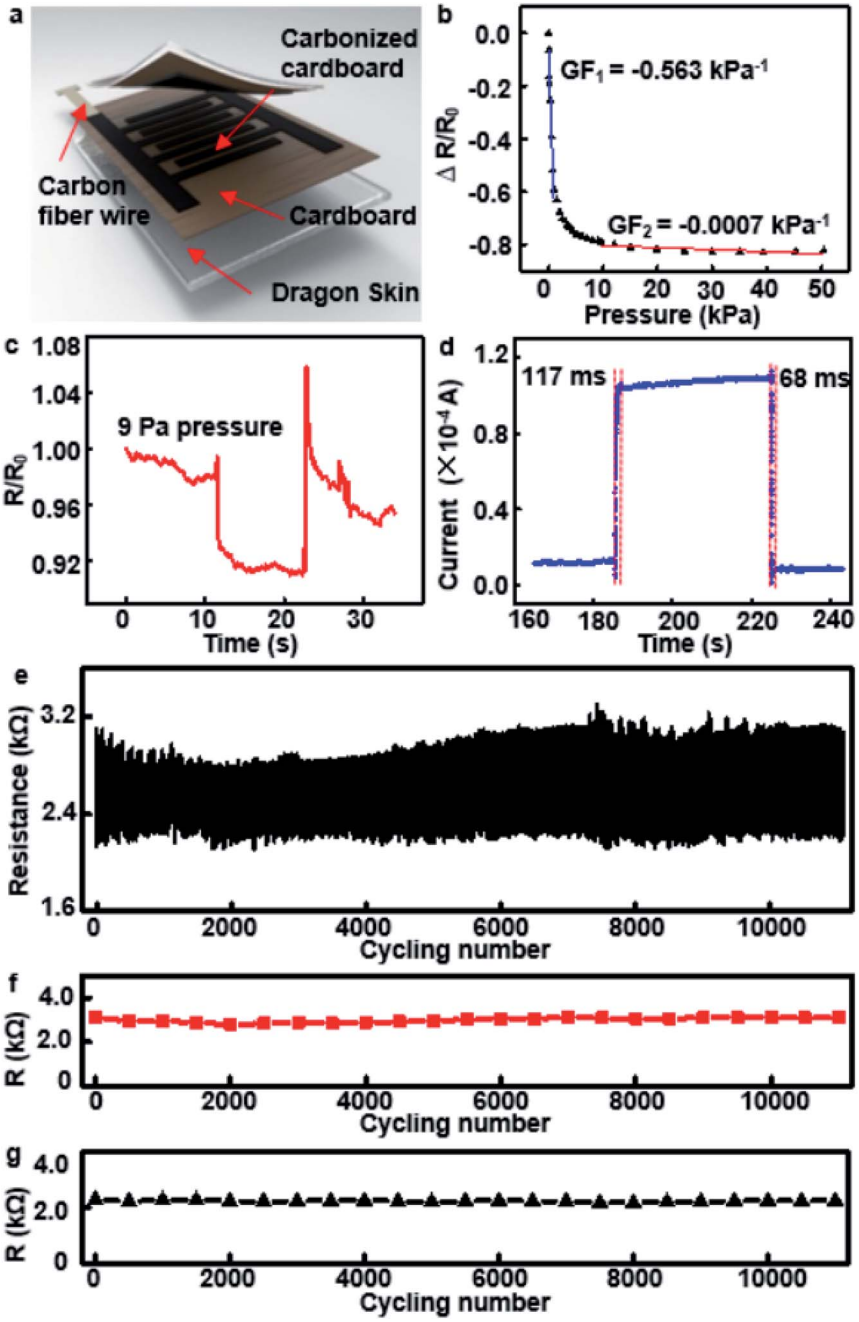

Fig. 3 Pressure-sensing and mechanical characterization of the carbonized cardboard pressure sensor. (a) A schematic of an LDW-fabricated pressure sensor. (b) The electrical response of the device at different applied pressures. (c) The minimum detectable pressure of the sensor. (d) The response/relaxation time for the pressure sensors. (e) Real-time electrical signals of the pressure sensor for over 11 000 loading/unloading cycles at an applied pressure of 10 kPa. (f) The resistance of the device without loading sampled at every 500 cycles. (g) The resistance of the device with loading sampled at every 500 cycles.

μm, due to the heat effect of the continuous wavelength laser, porous carbonaceous flakes which form stacked layers were found close to the grooves, as can be seen in the zoomed SEM image shown in Fig. 2b. Fig. 2c shows the morphology of the carbonized cardboard in the grooves. Carbon micro- and nano-particles were decorated on the surface of the carbonaceous flakes on the sidewalls of the grooves. To clearly observe the morphologies of the carbonaceous flakes at the grooves, the cross-sectional FE-SEM images at the grooves were captured and shown in Fig. 2d–f. Layered carbonaceous flakes with pores are observed. Unlike the compact structures of the pristine cardboard (Fig. S2d–f†), the carbonaceous flakes are separated, with particles decorated on them. Cardboard which is prepared by pressing several layers of paper together can be a good raw material for pressure sensors. When the laser was irradiated on the cardboard surface, the laser-delivered heat induced the

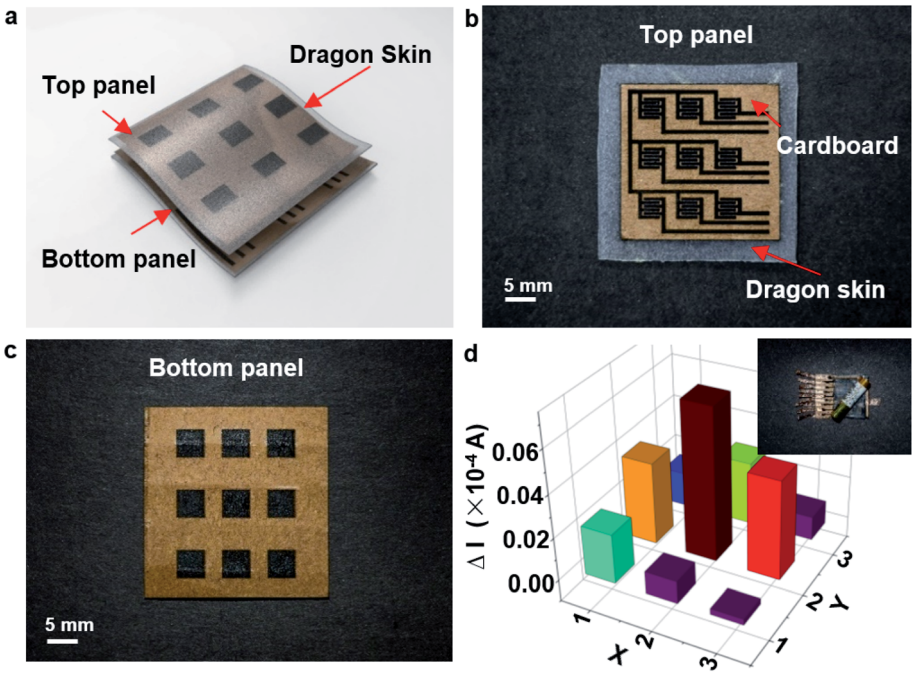

Fig. 4 A prototype pressure sensor array. (a) A schematic of an LDW-generated 3 × 3 array pressure sensor. (b) A photograph of the bottom panel of the sensor array. (c) A photograph of the top panel of the sensor array. (d) The electrical response of the sensor array upon the applying a AAA alkaline battery.

rapid carbonization of the cardboard, which causes the compacted paper layer scattered. The carbonization process might produce gases such as CO_2 and N_2,[37] which was confirmed by the following XPS analysis. The release of these gases could further lead to the formation of the gaps among the carbonaceous flakes.

The energy dispersive spectrometer (EDS) analysis of the cardboard shows that C and O are main elements of the cardboard in Fig. 2g. In addition, elements such as Ca, Si, Al, and Na are also found to exist in the cardboard. These presence of these elements is attributed to the $CaCO_3$, kaolin, and sulfate used in the preparation procedure of cardboard.[38,39] The ratio of the elements in the carbonized cardboard is listed in Table S1.† TEM was used to further examine the carbonized cardboard synthesized by LDW at 0.4 W with a scanning speed of 15 mm s^{-1}, as shown in Fig. 2h and i. Carbonaceous flakes decorated with carbon particles were observed. In the TEM images, the particles have sizes ranging from 35–112 nm.

The chemical composition of the carbonaceous flake was determined by XPS. Fig. 2j compares the XPS of the pristine and carbonized cardboard. For both spectrums, peaks assigned to C1s, O1s, and Ca2p are identified. The C/O atomic ratio is approximately the same before (70.57/23.32) and after (70.39/24.66) the LDW-induced carbonization. As shown in Fig. 2j, the presence of the N1s signal is more evident in the pristine cardboard and the intensity of the N1s peak decreases significantly after carbonization (Fig. S3a and b†), which proves that N_2 was released during the LDW processing. In addition, the complex XPS C1s spectra of carbonaceous materials was investigated and can be fitted by four components of 284.6, 285.2, 286.2 and 287.7 eV, ascribed to C=C, C–C, C–O and C=O, respectively.[40,41] The intensity of the C–O peak at 286.2 eV decreases after the carbonization process, indicating the possible release of CO_2 during the LDW processing (Fig. S3c and d†). Raman spectroscopy was adopted to study the quality of the LDW-carbonized cardboard. Fig. 2k illustrates the Raman spectra for the pristine and carbonized cardboard. No peaks were observed for the pristine cardboard within a wavenumber less than 3000 cm^{-1}. For the LDW-carbonized cardboard, peaks at 1350 and 1590 cm^{-1} attributed to the D- and G-bands of carbon were observed for the sample. The overlapping of the D- and G-bands indicates the low crystallinity of the carbonaceous flakes.

Sensing characteristic of the LDW pressure sensors

The LDW-carbonized cardboard was investigated as the electrodes of the pressure sensors. Fig. 3a is an exploded schematic view of the device. LDW-carbonized interdigitated electrodes (Fig. S4a†) were firstly formed on a piece of cardboard. Another carbonized layer with a rectangular shape (Fig. S4b†) was applied on top of the interdigitated electrodes to form the device. Upon pressing the sensor, the resistance between the interdigitated electrodes was measured. The corresponding electromechanical response of the device is shown in Fig. 3b. The application of the pressure causes the resistance of the device to decrease. The curve showing the relative resistance change ($\Delta R/R_0$) in response to pressure has two segments: one shows a fast decrease in $\Delta R/R_0$ at the low-pressure segment (<1 kPa) and the other shows a slow decrease in $\Delta R/R_0$ at the high-pressure segment (10–50 kPa). The corresponding sensitivities

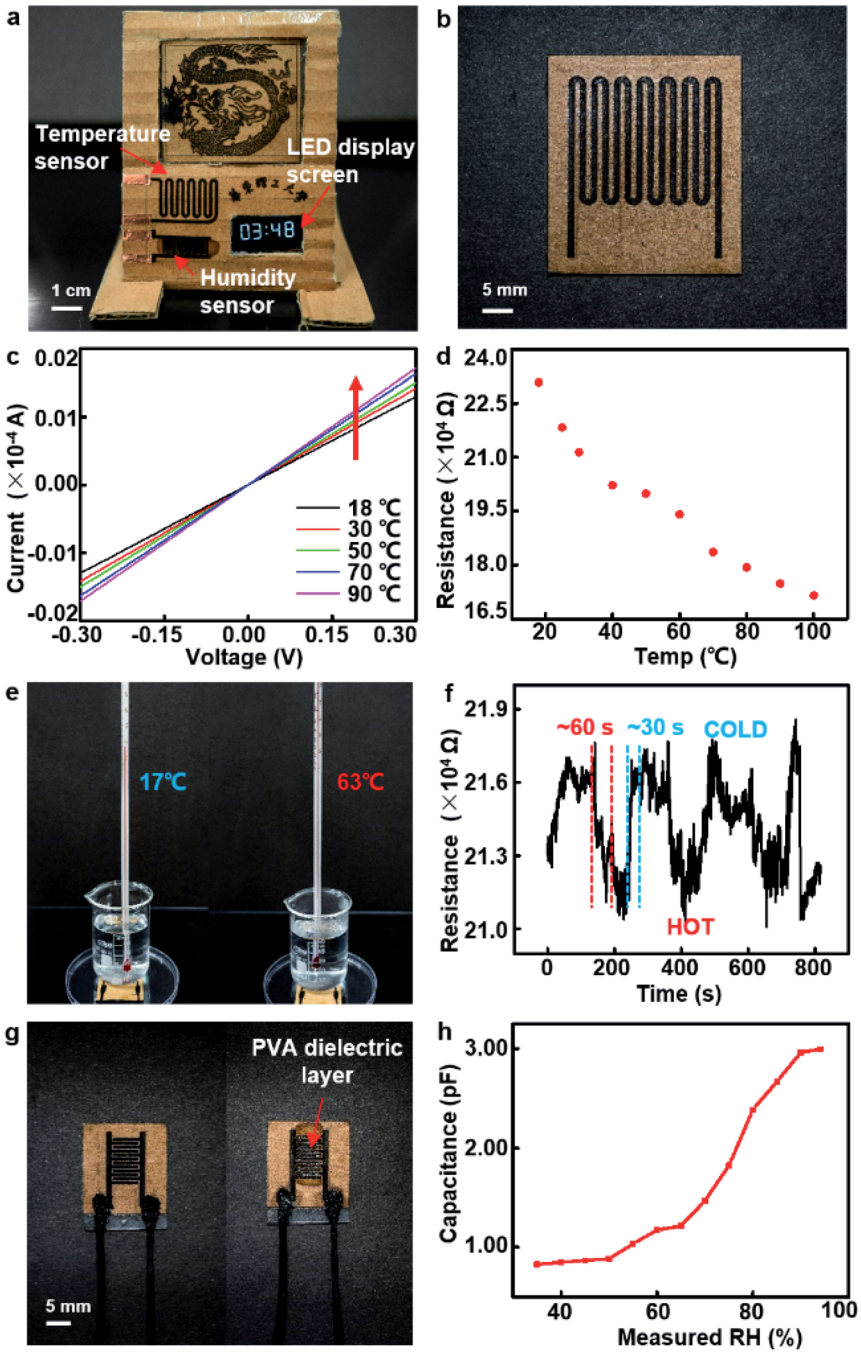

Fig. 5 Sensing behavior of the LDW-temperature and humidity sensors. (a) A photograph exhibiting a prototype of a home environment monitoring system based on cardboard integrated with LDW-fabricated temperature and humidity sensors. (b) A photograph of the resistive temperature sensor. (c) *I*–*V* curves of the temperature sensor within the temperature range of 18–100 °C. (d) Resistance variation in response to temperature change (18–100 °C). (e) A photograph showing the measurement of the beaker temperature using the temperature sensor. (f) Resistance change of the temperature sensor after contact with the beakers containing cold and hot water. (g) A photograph of an LDW-fabricated humidity sensor including an interdigitated electrode and a PVA dielectric layer. (h) Capacitance of the humidity sensor in response to environmental humidity variation.

for the low- and high-pressure segments are −0.563 and −0.0007 kPa^{-1}, respectively. The device has a sensing mode of pressure-induced resistance change, which could be attributed to the separated layered structures induced by LDW (Fig. 2d–f). As we have discussed above, cardboard consists of layered paper that is pressed together. The LDW-induced carbonization induces gas releasing, leading to the formation of carbon layers with separated layered structures. Upon pressing, the gaps among the carbonized layer are reduced and the conductivity of the device improves (Fig. S5†).

Fig. 3c shows the minimum pressure which the device is able to sense. The sensor can detect a piece of polydimethylsiloxane (1 g) placed on a sensing area of approximately 3 cm × 3 cm, which corresponds to the smallest detectable pressure of only 9 Pa and is comparable to the devices reported recently.[42,43] As illustrated in Fig. 3d, the response and relaxation times are 117 and 68 ms, respectively, which is obtained by applying and withdrawing a pressure of 6 kPa on the device. Fig. 3e illustrates the device stability for a cyclic test for more than 11 000 cycles at about 10 kPa. The resistance with and without loading for every 500 cycles was illustrated in Fig. 3f and g. Deviations of 10.58% (Fig. 3f) and 5.03% (Fig. 3g) in resistance are observed for the conditions with and without loading, respectively. The long-term stability of the device can be further improved in future research.

The reported sensing performance of the pressure device allows its application in monitoring of a variety of external stimuli. The LDW sensor is capable of detecting pressing force (Fig. S6a†) which is reflected by the conductivity enhancement of the device upon pressing (Fig. S6b†). The capability of the sensor to detect relatively smaller stimuli is confirmed by the measurement of signals generated by breathing, the radial pulse, and muscle movement. Fig. S7a and b† present the current change of the device attributed to the breathing of the volunteer. The detection of the pulse rate is conducted by applying a pressure sensor on the wrist of a student, as exhibited in Fig. S8a.† Fig. S8b† shows the corresponding pulse signal detected within 70 s, with a pulse rate of 71 pulses per-min for the student. Furthermore, the sensor can be used to detect the stimuli generated from the contraction and relaxation of muscles by attaching the device to the inner side of the forearm (Fig. S9a†). We obtained the muscle motion signal when the hand was clenched and relaxed within 30 s (Fig. S9b†). When the hand clenches, the muscles of the forearm contract, generating pressure to the sensor adhered to the muscle, which leads to the decrease of the resistance of the device. The signal returns to the initial state after relaxation.

The investigation of the carbonaceous pressure sensors is not limited to the detection of human motion generated stimuli. A 3 × 3 pixel array of LDW pressure sensors was developed to measure the pressure distribution generated by external stimuli, as schematically illustrated in Fig. 4a. The sensor array has a pixel area of 5 mm × 5 mm. The carbonized array of the interdigitated electrodes (Fig. 4b) and the top carbonized layer (Fig. 4c) were both prepared by the LDW carbonization process on cardboard. To facilitate the measurement, ecoflex was used as the substrate for accommodating the top and the bottom electrodes. An Arduino electronic platform was built to characterize the pressure array, which is capable of measuring the 3 × 3 square blocks. The ability of the pressure sensor array in detecting pressure distribution is illustrated in Fig. 4d. Pressures were applied to the sensors *via* an AAA alkaline battery laid on the surface of the device. The corresponding electrical signal changes are recorded in Fig. 4d.

Sensing behavior of the LDW-temperature and humidity sensors

Human quality of life and working efficiency are affected by the indoor environment, especially thermal comfort and humidity. An indoor monitoring system is quite important for the indoor environment control system to provide a comfortable physical environment for humans. Herein, the LDW-fabricated temperature and humidity sensors are investigated for this potential application. A cardboard-based indoor monitoring prototype is demonstrated, as shown in Fig. 5a. The device consists of an LDW-induced Chinese dragon, a temperature sensor, a humidity sensor, a clock, and an Arduino electronic platform. The temperature and the humidity detected by the sensors can be read by the Arduino electronic platform (Fig. S10†) and displayed on the LED screen.

Fig. 5b illustrates the device configuration of the temperature sensor, with a serpentine trace of carbonized cardboard by LDW. Fig. 5c shows the *I*–*V* curves of the sensor upon heating from a temperature of 18 to 100 °C (plotting step is 20 °C, for clarity) at a fixed applied voltage of 0.3 V. The LDW carbonized cardboard has a typical negative temperature coefficient demonstrated by the heating-induced conductivity increase (Fig. 5c), which is similar to that of other reported carbon-based materials.[44–46] The resistances of the sensor at different temperatures were sampled and plotted in Fig. 5d. The resistance *versus* temperature is roughly linear, with a sensitivity of −0.00293/°C for the device. The sensitivity of the carbonized cardboard temperature sensor fabricated by LDW processing is comparable to other recently reported devices obtained by printing, etching and laser processing method.[47,48] The temperature sensor was employed to measure the temperature for cold (17 °C) and hot water (63 °C) in beakers (Fig. 5e). Fig. 5f illustrates the resistances change of the temperature sensor when the beakers containing the cold and hot water were put on the device. The cold water causes the resistance of the device to increase, while hot water causes the resistance to decrease. As shown in Fig. 5f, the response time for the sensor is ∼30 and 60 s for detecting the cold and hot water, respectively. The relatively slow response time could be ascribed to the thermal conduction process among the water, beaker, and sensor, as well as the low thermal conductivity of the cardboard.

It has been proven that PVA is a promising active material for humidity sensors since it offers advantages including high sensitivity, fast response, and low cost, *etc.*[49,50] The backbone of the polyelectrolyte is typically hydrophobic, while the electrolytic group is soluble in water. When water is absorbed on these porous membranes, the porous membranes serves as an aqueous phase electrolyte material. The ions dissolved in the aqueous layer formed by absorption become conductive carriers. Due to its high mobility, the conductivity of the film increases as humidity increases.[51] As shown in Fig. 5g, the capacitive humidity sensor was fabricated by coating of LDW-induced interdigitated electrodes with a layer of PVA as the sensing layer. Fig. 5h depicts the capacitance change of the humidity sensor response to different environmental Relative Humidity (RH). The humidity device demonstrates a sensitivity

of 36.75 fF per %RH in a range between 35% and 94% RH. The LDW-fabricated humidity sensor has a fairly good stability of the humidity sensing in a humid environment, as shown in Fig. S11.†

4. Conclusions

In summary, an LDW method was developed for direct patterning of carbonaceous sensors on cardboard for human health monitoring and indoor environment monitoring. LDW induces layered porous carbon on the cardboard, which enables the fabrication of sensors for measuring mechanical stimuli, temperature, and humidity. The LDW-fabricated pressure sensors on cardboard have a sensitivity of $-0.563\ kPa^{-1}$, a broad detecting range from 9 Pa to 50 kPa, fast response/relaxation speed (117 ms/68 ms), and a good durability (11 000 cycles). A 3×3 pixel pressure sensing array of carbonized cardboard was further fabricated for the application in electronic skins. The carbonaceous sensors on cardboard can be fabricated as resistive temperature and capacitive humidity sensors for indoor environment monitoring. The resistive temperature has a sensitivity of $-0.00293/°C$, while the humidity sensor provides a sensitivity of 36.75 fF per %RH.

Conflicts of interest

There are no conflicts to declare.

Acknowledgements

This project is supported by National Key Research and Development Program of China (No. 2018YFB1105400), National Natural Science Foundation of China (Grant No. 51705154, 51835003 and 61804054), Joint Fund of Ministry of Education of China for Equipment Preresearch (Grant No. 6141A02022136), Shanghai Program for Professor of Special Appointment (Eastern Scholar) at Shanghai Institutions of Higher Learning, Shanghai Rising-Star Program (A type) (Grant No. 18QA1401300), and Shanghai Sailing Program 17YF1403300.

References

1 D. Silvera-Tawil, D. Rye and M. Velonaki, *Robot. Auton. Syst.*, 2015, **63**(Part 3), 230–243.
2 A. Chortos, J. Liu and Z. A. Bao, *Nat. Mater.*, 2016, **15**, 937–950.
3 G. Mattana, T. Kinkeldei, D. Leuenberger, C. Ataman, J. J. Ruan, F. Molina-Lopez, A. V. Quintero, G. Nisato, G. Tröster, D. Briand and N. F. d. Rooij, *IEEE Sens. J.*, 2013, **13**, 3901–3909.
4 S. Jung, J. H. Kim, J. Kim, S. Choi, J. Lee, I. Park, T. Hyeon and D.-H. Kim, *Adv. Mater.*, 2014, **26**, 4825–4830.
5 Y.-C. Lai, B.-W. Ye, C.-F. Lu, C.-T. Chen, M.-H. Jao, W.-F. Su, W.-Y. Hung, T.-Y. Lin and Y.-F. Chen, *Adv. Funct. Mater.*, 2016, **26**, 1286–1295.
6 Z. Chen, Z. Wang, X. Li, Y. Lin, N. Luo, M. Long, N. Zhao and J.-B. Xu, *ACS Nano*, 2017, **11**, 4507–4513.
7 D. H. Ho, Q. Sun, S. Y. Kim, J. T. Han, D. H. Kim and J. H. Cho, *Adv. Mater.*, 2016, **28**, 2601–2608.
8 L. Nela, J. Tang, Q. Cao, G. Tulevski and S.-J. Han, *Nano Lett.*, 2018, **18**, 2054–2059.
9 T. Q. Trung and N.-E. Lee, *Adv. Mater.*, 2016, **28**, 4338–4372.
10 R. Pitarma, G. Marques and B. R. Ferreira, *J. Med. Syst.*, 2016, **41**, 23.
11 A. Chortos and Z. Bao, *Mater. Today*, 2014, **17**, 321–331.
12 H.-K. Chang, E. Choi and J. Park, *Lab Chip*, 2016, **16**, 700–708.
13 X. Wang and C. Yu, *J. Mater. Res.*, 2020, **35**, 940–948.
14 S. Y. Kim, S. Park, H. W. Park, D. H. Park, Y. Jeong and D. H. Kim, *Adv. Mater.*, 2015, **27**, 4178–4185.
15 K. Xia, C. Wang, M. Jian, Q. Wang and Y. Zhang, *Nano Res.*, 2018, **11**, 1124–1134.
16 Y. Yang, S. Ding, T. Araki, J. Jiu, T. Sugahara, J. Wang, J. Vanfleteren, T. Sekitani and K. Suganuma, *Nano Res.*, 2016, **9**, 401–414.
17 Y. Ma, N. Liu, L. Li, X. Hu, Z. Zou, J. Wang, S. Luo and Y. Gao, *Nat. Commun.*, 2017, **8**, 1207.
18 Y. Panraksa, W. Siangproh, T. Khampieng, O. Chailapakul and A. Apilux, *Talanta*, 2018, **178**, 1017–1023.
19 P. R. Tortorich, H. Shamkhalichenar and J.-W. Choi, *Appl. Sci.*, 2018, **8**, 288.
20 Y. He, Q. Gao, W.-B. Wu, J. Nie and J.-Z. Fu, *Micromachines*, 2016, **7**, 108.
21 V. Malyarchuk, F. Hua, N. H. Mack, V. T. Velasquez, J. O. White, R. G. Nuzzo and J. A. Rogers, *Opt. Express*, 2005, **13**, 5669–5675.
22 X. Xiao, L. Yuan, J. Zhong, T. Ding, Y. Liu, Z. Cai, Y. Rong, H. Han, J. Zhou and Z. L. Wang, *Adv. Mater.*, 2011, **23**, 5440–5444.
23 K. R. R. Venkata, A. K. Venkata, P. S. Karthik and P. S. Surya, *RSC Adv.*, 2015, **5**, 77760–77790.
24 W. Zhou, S. Bai, Y. Ma, D. Ma, T. Hou, X. Shi and A. Hu, *ACS Appl. Mater. Interfaces*, 2016, **8**, 24887–24892.
25 M. F. El-Kady, V. Strong, S. Dubin and R. B. Kaner, *Science*, 2012, **335**, 1326.
26 H. Tian, Y. Shu, X.-F. Wang, M. A. Mohammad, Z. Bie, Q.-Y. Xie, C. Li, W.-T. Mi, Y. Yang and T.-L. Ren, *Sci. Rep.*, 2015, **5**, 8603.
27 Y. Qiao, Y. Wang, H. Tian, M. Li, J. Jian, Y. Wei, Y. Tian, D.-Y. Wang, Y. Pang, X. Geng, X. Wang, Y. Zhao, H. Wang, N. Deng, M. Jian, Y. Zhang, R. Liang, Y. Yang and T.-L. Ren, *ACS Nano*, 2018, **12**, 8839–8846.
28 S. Luo, P. T. Hoang and T. Liu, *Carbon*, 2016, **96**, 522–531.
29 R. Rahimi, M. Ochoa and B. Ziaie, *ACS Appl. Mater. Interfaces*, 2016, **8**, 16907–16913.
30 Y. Gao, Q. Li, R. Wu, J. Sha, Y. Lu and F. Xuan, *Adv. Funct. Mater.*, 2019, **29**, 1806786.
31 D. Wu, L. Deng, X. Mei, K. S. Teh, W. Cai, Q. Tan, Y. Zhao, L. Wang, L. Zhao, G. Luo, D. Sun and L. Lin, *Sens. Actuators, A*, 2017, **267**, 327–333.
32 A. Stepanov, E. Saukkonen and H. Piili, *Phys. Procedia*, 2015, **78**, 138–146.

33 T.-N. Ye, W.-J. Feng, B. Zhang, M. Xu, L.-B. Lv, J. Su, X. Wei, K.-X. Wang, X.-H. Li and J.-S. Chen, *J. Mater. Chem. A*, 2015, **3**, 13926–13932.
34 S. Chen, Y. Song, D. Ding, Z. Ling and F. Xu, *Adv. Funct. Mater.*, 2018, **28**, 1802547.
35 L. E. Larrondo and P. Lepoutre, *J. Colloid Interface Sci.*, 1992, **152**, 33–40.
36 E. Gastaldi, P. Chalier, A. Guillemin and N. Gontard, *Colloids Surf., A*, 2007, **301**, 301–310.
37 W. R. de Araujo, C. M. R. Frasson, W. A. Ameku, J. R. Silva, L. Angnes and T. R. L. C. Paixão, *Angew. Chem.*, 2017, **56**, 15113–15117.
38 W. M. Bundy and J. N. Ishley, *Appl. Clay Sci.*, 1991, **5**, 397–420.
39 Y. Tang, D. Zhou, J. Zhang and X. Zhu, *Dig. J. Nanomater. Biostructures*, 2013, **8**, 1699–1710.
40 X. Xiang, E. Liu, Z. Huang, H. Shen, Y. Tian, C. Xiao, J. Yang and Z. Mao, *J. Solid State Electrochem.*, 2011, **15**, 2667–2674.
41 S. Kaciulis, *Surf. Interface Anal.*, 2012, **44**, 1155–1161.
42 C. Lu, Y. Gao, G. Yu, M. Xu, J. Tan and F. Xuan, *Sens. Actuators, A*, 2018, **281**, 124–129.
43 Y. Pang, K. Zhang, Z. Yang, S. Jiang, Z. Ju, Y. Li, X. Wang, D. Wang, M. Jian, Y. Zhang, R. Liang, H. Tian, Y. Yang and T.-L. Ren, *ACS Nano*, 2018, **12**, 2346–2354.
44 M. Mohiuddin and S. Van Hoa, *Nanoscale Res. Lett.*, 2011, **6**, 419.
45 S. Zhao, D. Lou, P. Zhan, G. Li, K. Dai, J. Guo, G. Zheng, C. Liu, C. Shen and Z. Guo, *J. Mater. Chem. C*, 2017, **5**, 8233–8242.
46 J. X. Li, *Adv. Mater. Res.*, 2011, **301–303**, 1128–1132.
47 C.-Y. Lee, C.-H. Lin and Y.-M. Lo, *Sensors*, 2011, **11**, 3706.
48 S. Harada, W. Honda, T. Arie, S. Akita and K. Takei, *ACS Nano*, 2014, **8**, 3921–3927.
49 M.-R. Yang and K.-S. Chen, *Sens. Actuators, B*, 1998, **49**, 240–247.
50 Y. Li, M. J. Yang, N. Camaioni and G. Casalbore-Miceli, *Sens. Actuators, B*, 2001, **77**, 625–631.
51 Z. Chen and C. Lu, *Sensor Lett.*, 2005, **3**, 274–295.